Applied Surface Science 465 (2019) 201–206

Contents lists available at ScienceDirect

Applied Surface Science

journal homepage: www.elsevier.com/locate/apsusc

Full Length Article

Shape transitions of Cu_3Si islands grown on Si(1 1 1) and Si(1 0 0)

E.S. Srinadhu[a], J.E. Harriss[b], C.E. Sosolik[b,*]

[a] Lam Research Corporation, Fremont, CA 94538, USA
[b] Department of Physics and Astronomy, Clemson University, Clemson, SC 29634, USA

ARTICLE INFO

Keywords:
Cu silicides
Cu_3Si
Nanowires
Triangles
Nanorectangles
Strain induced shape transition
Trapezoid

ABSTRACT

In this paper, we report on the formation of epitaxial copper silicide (Cu_3Si) islands and their subsequent shape transitions on Si(1 1 1) and Si(1 0 0) substrates. For island growth on Si(1 1 1), equilateral triangles have been found to grow up to a critical size, beyond which a shape transition to trapezoid occurs. Similarly, on a Si(1 0 0) surface, square islands are observed which transition to rectangular islands and long nanowires. Initial growth on all substrates appears to be contingent on void formation that is tied directly to sustained high temperature processing of the samples. Overall, the island area and density are consistent with diffusion-driven growth and energetic barriers extracted from temperature-dependent data are in line with those seen in other studies.

1. Introduction

Understanding the fundamental interactions of metals with silicon and the role of those interactions in the growth of silicides is an area of research that has direct applications within the semiconductor industry [1–3]. For example, metal silicides are used as diffusion barriers and ohmic contacts in silicon-based devices, highlighting the need to understand their growth behavior on the nanoscale [4,5]. In the work presented here, we study copper in the presence of an ultrathin SiO_2 layer. Copper is a key interconnect material in electronics due to its low resistivity and excellent electromigration resistance [6–8]. Similarly, layers of SiO_2 are routinely used in modern multilevel metallization structures as the effective diffusive barrier to isolate interconnect lines and to separate active devices from contacted metals [9,10]. The growth mechanisms for Cu silicides in the presence of an ultrathin SiO_2 barrier, however, have not been fully explored. One system in particular, Cu_3Si, is the focus of our study [11–14].

Recent interest in Cu_3Si stems from its possible use in energy storage applications, such as batteries and solar cells [15,16]. For example, Kaiqi et al. investigated the use of Cu_3Si in battery anodes and showed that an excellent electrochemical performance was obtained for a Si-Cu_3Si-Cu composite electrode structure [17]. Also, it has been shown recently that Cu_3Si nanowires exhibit superior field-emission properties and can serve as highly efficient anti-reflective layers and as an effective catalyst in reactions [18,19].

In considering growth mechanisms for silicides, we note that in general, layer-by-layer epitaxial growth is feasible in systems that are unstrained, i.e. where the lattice constant of the epilayer matches that of the substrate on which it is grown. When there is a mismatch in the lattice constants, however, the growth of islands or nanodots becomes feasible. For example, in Ge/Si(0 0 1) and InAs/GaAs(0 0 1), a symmetric lattice mismatch leads to strained growth that is relaxed through nanostructure formation [20–22]. Strain relief can also be achieved through a transition in the shapes of the nanoislands that are formed. In this case, islands grown below a critical size will have a compact symmetric shape, whereas larger sized islands will adopt a long thin wire shape to allow for a further relaxation of the island's stress. Such transitions have been observed in systems like Au_4Si/Si(1 1 1), $CoSi_2$/Si (1 0 0) and Ti/Si(1 1 1) [23–26], which all exhibit a form of elongated island growth that is consistent with the strain-driven shape transition" models put forward in Refs. [27,28]. We note that the approach of Ref. [28], which involves facet growth and hut-like clusters in coherently strained islands, could be applied with some validity to our data presented here. However, here, for the purpose of our discussion we focus on Ref. [27].

For nanowires in particular, an anisotropic lattice mismatch can lead to their preferential growth. In silicide systems, nanowire shapes are believed to result from a small mismatch (<1%) in the length direction and a large mismatch (> 5%) in the width direction of the nanowire. For example rare-earth metals like Sm, Dy, Er, Pt, and Gd deposited on heated Si(1 0 0) substrates form self-assembled metal disilicide nanowires from such an anisotropic lattice mismatch [12,29–38].

A more complex growth process described by He et al. and applied to a range of transition metals on silicon is endotaxial growth. This mechanism involves epitaxial growth into the substrate without an

* Corresponding author.
E-mail addresses: esrinad@g.clemson.edu (E.S. Srinadhu), james4@clemson.edu (J.E. Harriss), sosolik@clemson.edu (C.E. Sosolik).

https://doi.org/10.1016/j.apsusc.2018.09.018
Received 9 May 2018; Received in revised form 15 August 2018; Accepted 3 September 2018
Available online 18 September 2018
0169-4332/

anisotropic lattice mismatch. A twinning relationship between the substrate and silicide breaks the symmetry of the surface and leads to an asymmetric growth of islands. A variety of metal silicides like $CoSi_2$,$TiSi_2$,$FeSi_2$ on Si(1 0 0) have been grown by this method [39–41].

The organization of this paper is as follows. In Section 2 we describe our experimental setup and the preparation and characterization steps for our ultrathin SiO_2 layers and subsequent Cu depositions. The results of these depositions, analyzed primarily through scanning electron microscope (SEM) images, are presented and discussed in Section 3. A summary of our data and results are included in Section 4.

2. Experiment

Single crystal, 3-inch diameter, Si wafers with resistivities of 1–10 Ω cm were used in the work presented here. Specifically, boron-doped p-type Si(1 1 1) and Si(1 0 0) and phosphorous-doped n-type Si(1 1 1) wafers were used. All wafers were prepared initially using a standard RCA clean procedure, which involved cleaning in a chemical bath (1:1:5 solution of $NH_4OH + H_2O_2 + H_2O$) for five minutes under ultrasonic agitation. The cleaned surface was then etched with dilute 1% HF for two minutes and triple-rinsed in deionized water for six minutes to remove any native oxide. Following this cleaning, the oxidation, anneal, and metal deposition steps illustrated in Fig. 1 and discussed below were used to grow Cu_3Si nanostructures. First, an ultrathin thermal oxide layer (1.5 ± 0.05 nm) was grown onto the Si surfaces using dry oxidation in a furnace at 200 °C for 2 h. Measurements to verify the resulting oxide thickness were made at five locations on each wafer (center and 4 corners) using a Sopra GES-5E spectroscopic ellipsometer. The oxide-covered Si wafers were then diced into 10 mm × 10 mm squares for mounting onto Omicron-style sample platens that could be load-locked into our deposition chamber.

Within this chamber the SiO_2/Si substrates were annealed overnight (10–12 h) using a HeatWave Labs, Inc. UHV button heater at a temperature of 500 °C ± 25 °C to remove surface carbonaceous impurities. This annealing also led to the decomposition of the ultrathin SiO_2 and the formation of voids at defect sites (see, *e.g.* Fig. 3), which could serve as nucleation centers for the growth of Cu_3Si nanostructures. Thin Cu films were deposited onto the diced SiO_2/Si samples at elevated temperatures (450–550 °C) using an electron beam evaporator (McAllister Technical Services) at a pressure of 5×10^{-6} Torr. The deposition times ranged from 1 min. to 6 min. after which the samples were removed from the deposition chamber and imaged with the SEM (Hitachi S4800). A typical SEM image of Cu_3Si nanostructures that resulted from our preparation and growth steps is shown in Fig. 2. To verify the chemical morphology of the Cu_3Si nanostructures, X-ray diffraction studies were also performed using a Rigaku diffractometer.

3. Results and discussion

As we noted in the previous section and illustrate in Fig. 1, our SiO_2/Si substrates were annealed prior to the deposition of Cu. Here we discuss the results of both the annealing and deposition steps as they relate to the formation of Cu_3Si nanostructures. In particular, we focus on the development of nucleation centers or voids at the surface, the deposition of Cu at low temperatures ($T < 450$ °C), and the deposition of Cu and growth of nanostructures in an optimal temperature range (450 °C $< T <$ 600 °C).

First, it is known from prior studies that an annealing step is required to successfully form Cu_3Si nanostructures on SiO_2/Si [11,13,42]. We took a similar route in this work, annealing our prepared SiO_2/Si samples at 500 °C overnight for 10–12 h in our vacuum system. To understand the role of this step in the later formation of nanostructures, we prepared a subset of samples for SEM analysis that were annealed at temperatures of 500–550 °C. The SEM images revealed a variation in the density of voids at the sample surfaces which can be seen from the three representative images shown in Fig. 3. An examination of these voids with energy-dispersive X-ray spectroscopy (EDX) revealed them to be bare Si regions of sizes 2–18 μm^2. Across this narrow range, the data in Fig. 3 show that the density of voids grows linearly with temperature, with densities in the 10^5–10^6 cm^{-2} range. Although it is likely that smaller void regions are present below the resolving limit of our SEM analysis, the presence of voids and their distinct dependence on

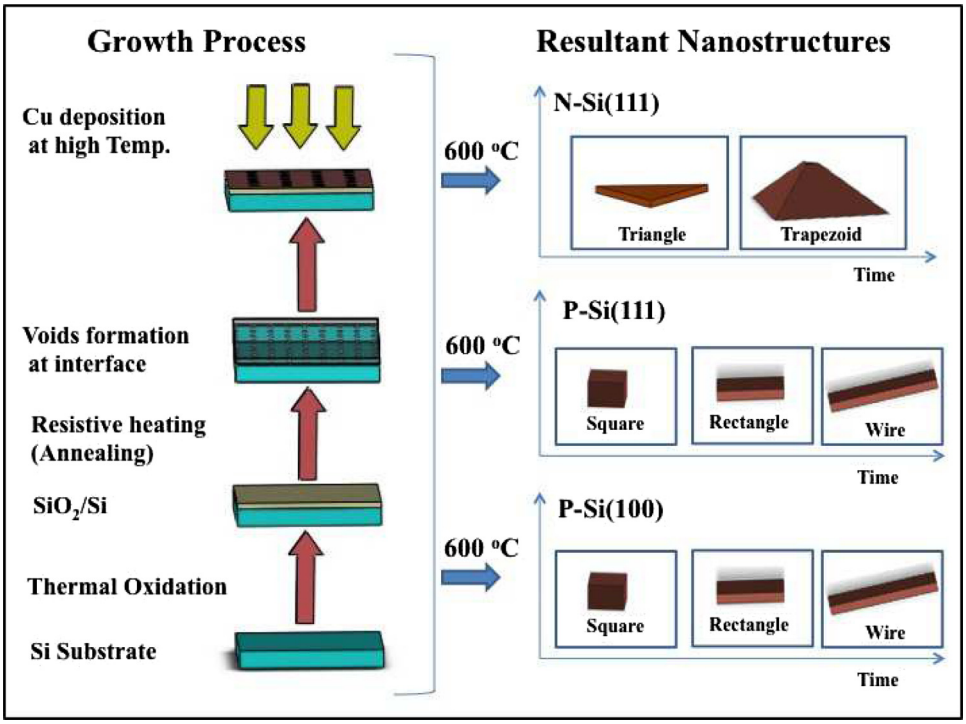

Fig. 1. Illustration of Cu_3Si growth process on our prepared ultrathin SiO_2/Si wafers. Left side shows oxidation, annealing, and deposition steps. Right side shows resultant Cu_3Si structures formed for different Si orientations and doping.

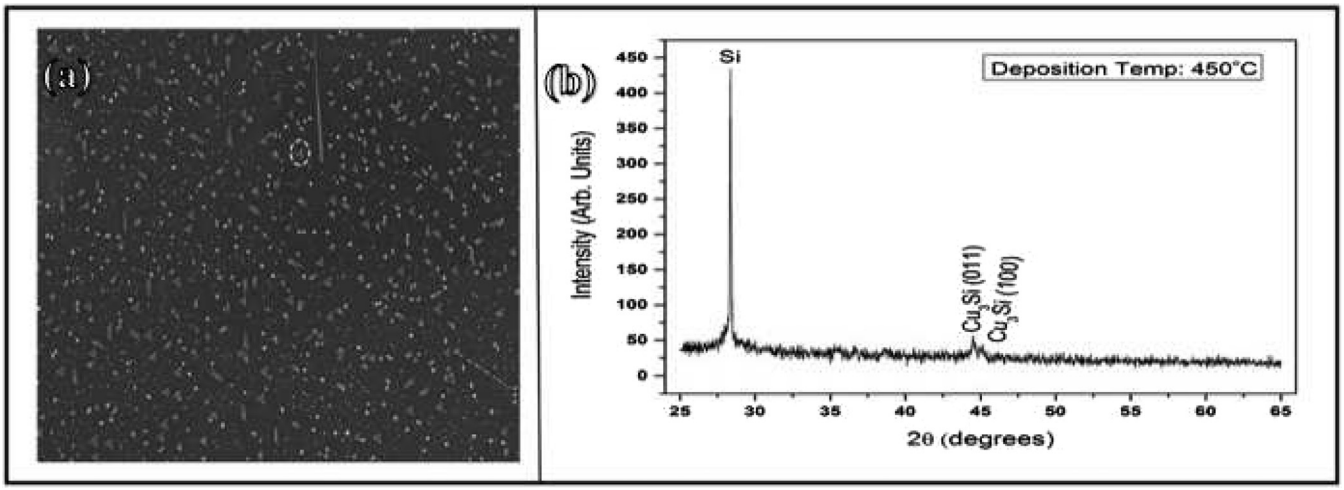

Fig. 2. Typical results showing (a) SEM and (b) X-ray diffraction data obtained for Cu_3Si islands grown on SiO_2/Si(1 1 1) at 450 °C. Dotted circle in SEM image indicates location where X-ray data were taken.

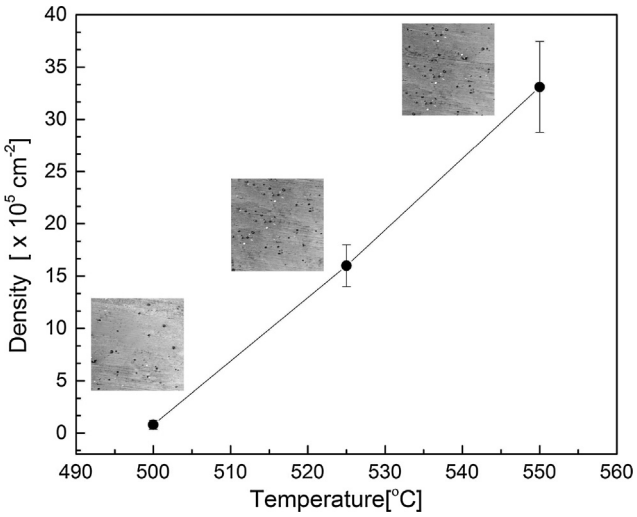

Fig. 3. Density of voids formed on SiO_2/Si(1 1 1) substrates as function of the overnight (10–12 h) annealing temperature. The three SEM images are representative of the voids seen at each annealing temperature with each image being 2500 μm^2 in area. The error bars represent a standard error of 10^3 voids.

temperature indicates that they may play an important role in Cu_3Si nanostructure formation within our optimal temperature range.

The deposition of Cu on our prepared and annealed substrates at room temperature and below approximately 450 °C resulted in the growth of features with irregular shapes. For example Fig. 2(a) shows a distribution of such features at this boundary point ($T \sim 450$ °C). X-ray data taken here (Fig. 2(b)) reveal that the formation of the Cu_3Si phase is already underway. Specifically, the peaks in the data near 45° show a composition of 24.5% Si and 75.5% Cu, respectively.

Above 450 °C, we find that Cu deposition leads to Cu_3Si nanostructure growth in regular, distinct shapes. Examples are shown in Fig. 4 for a constant deposition (~5 ML) of Cu on n- and p-type Si substrates. On n-type Si(1 1 1) (Fig. 4(a)) small equilateral triangular islands are observed, reflecting the threefold symmetry of the substrate, whereas on p-type Si(1 1 1) (Fig. 4(b)) long nanowires are observed. Both rectangular islands and nanowires are observed on p-type Si(1 0 0) as the temperature is varied from 500 to 600 °C (Fig. 4(c) and (d)). We note that discussions based on our SEM images here and below will assume that there is defect-free, epitaxial island growth. Additional measurements of 3D structure, such as TEM or AFM, are required to validate this assumption.

If we focus in more detail on nanoisland formation on the p-type (1 0 0) substrate, we can see (Fig. 5(a)) that the islands are square in shape reflecting the fourfold symmetry of the substrate. There is a transition to elongated rectangles (Fig. 5(b)) followed by the formation of long thin or quasi one-dimensional nanowires (Fig. 5(c)). For this experiment, nanowires with aspect ratios as large as ~20:1 were observed. Since there was a distribution of nano-islands of all sizes on the growth surface, islands of approximately the same size and area were averaged to obtain the curve shown in Fig. 5(d). Each point on this curve represents an average of ~100 islands. Based on the length-to-width ratio of the growing islands, which increases with the island area, it appears that when the island area is larger than a critical size, the growth tends to occur preferentially along certain directions.

A similar evaluation of nanoisland formation on the p-type (1 1 1) substrate is shown in Fig. 6. The observed behavior is similar to that seen on the (1 0 0) surface, with a shape transition from nano-rectangles to long thin wires with aspect ratios as large as ~9:1. In contrast, however, the nanoislands grown on the n-type (1 1 1) substrate were triangular in shape or essentially zero-dimensional quantum dots as shown in Fig. 7(a). This corresponds to the threefold symmetry of the substrate with a transition to trapezoidal shapes (Fig. 7(b)).

The shape transitions we observed can be explained by the model proposed by Tersoff and Tromp which uses energetic and kinetic constraints to predict the macroscopic characteristics such as aspect ratio for epitaxial nanoislands [27]. Their model requires well-separated islands and continuous deposition at high temperatures, ideally our experimental conditions, to study island elongation. The model states that below a certain critical size, the islands are symmetrical in shape, and beyond the critical size, the islands undergo a transition to an elongated shape for stress mitigation. An island under stress exerts a force on the substrate surface, which elastically distorts the substrate and lowers the energy of the islands at the cost of substrate strain. The optimal trade-off between surface energy and strain is obtained by minimization of the energy-to-volume ratio. Atoms deposited on the surface will diffuse to existing islands and are more likely to attach to the edges than to diffuse to the island's top surface. As a result, island heights grow slowly compared to lateral dimension (length and width), and thus the heights may be treated as approximately constant. A compact shape of equal length and width is considered stable for the islands until the dimensions exceed the critical size, and the compact shape becomes unstable giving a transition to elongated shapes. During the elongation phase, island lengths tend to increase while the island widths decrease asymptotically and trend back toward the critical value. This general feature of bifurcation in the shape at critical size points is represented in

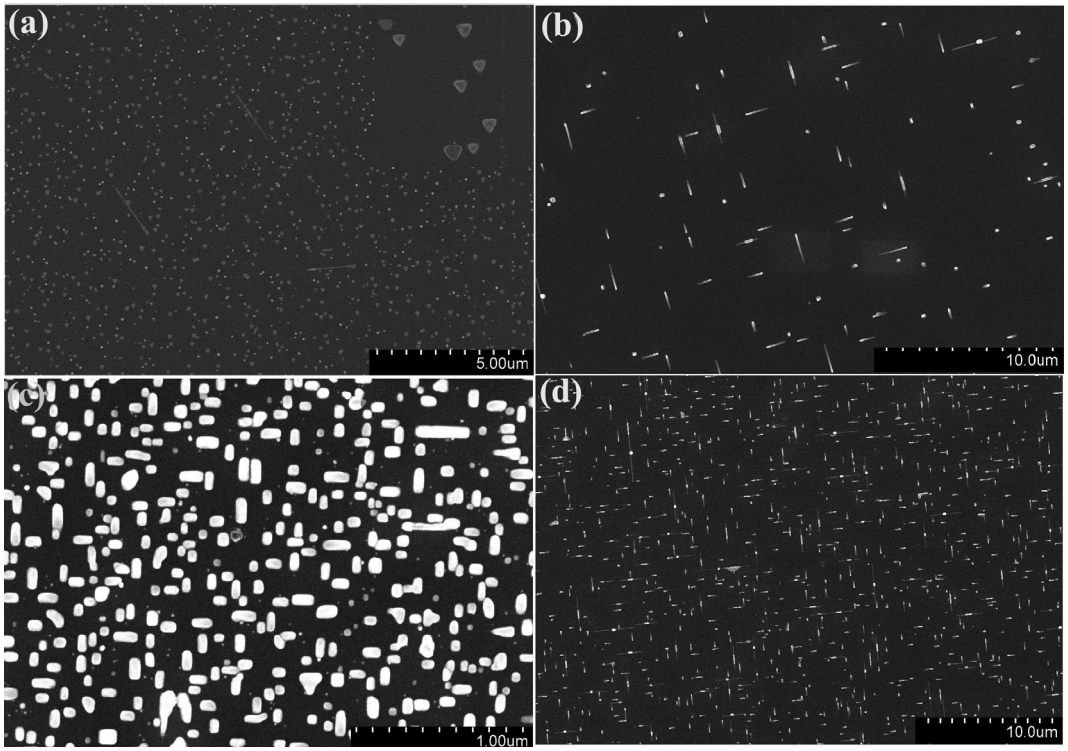

Fig. 4. SEM images obtained from ~5 ML depositions of Cu onto heated SiO_2/Si substrates: (a) n-Si(1 1 1) at 600 °C (inset shows close-up of triangular nanostructures), (b) p-Si(1 1 1) at 600 °C, (c) p-Si(1 0 0) at 550 °C, and (d) p-Si(1 0 0) at 600 °C.

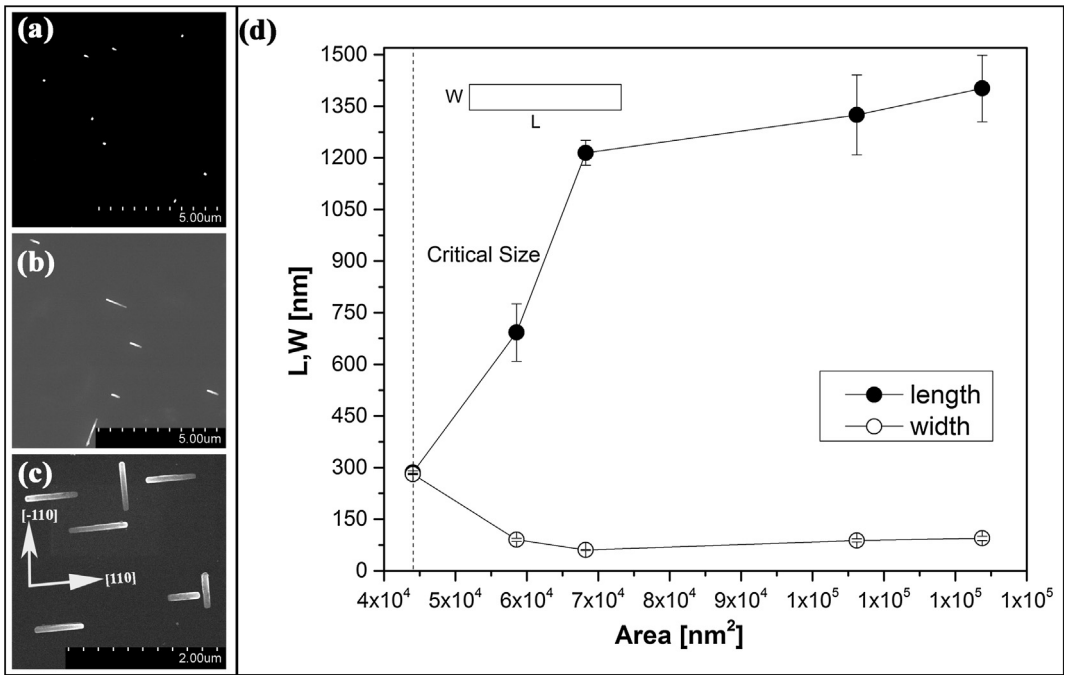

Fig. 5. Three stages of Cu_3Si island growth on a p-type Si(1 0 0) substrate as seen with SEM: (a) square islands, (b) rectangular islands, and (c) long, wire-shaped islands. Panel (d) shows the dependence of both island length L(closed circles) and width W(open circles) on the island surface area.

our data as the dotted lines shown Figs. 5–7(d).

The overall density and individual areas of the various Cu_3Si islands formed on our substrates was examined in detail over the temperature range of 500–600 °C, with the results plotted in Fig. 8. Here the densities are shown as an Arrhenius plot, allowing for the determination of the activation energies for the island growth process. We find these to be 1.17 eV (n-type Si(1 1 1)), 1.02 eV (p-type Si(1 1 1)) and 0.94 eV (p-type Si(1 0 0)) which matches closely the values reported elsewhere [11,43]. In particular, we note that this range of values for Cu diffusion in silicide growth are consistent with the case of initially incomplete condensation or incomplete condensation [11,44]. The inset of Fig. 8 shows the average island area across the various substrates, which increases by more than an order of magnitude across our temperature range. These data are shown as a function of deposition time in Fig. 9.

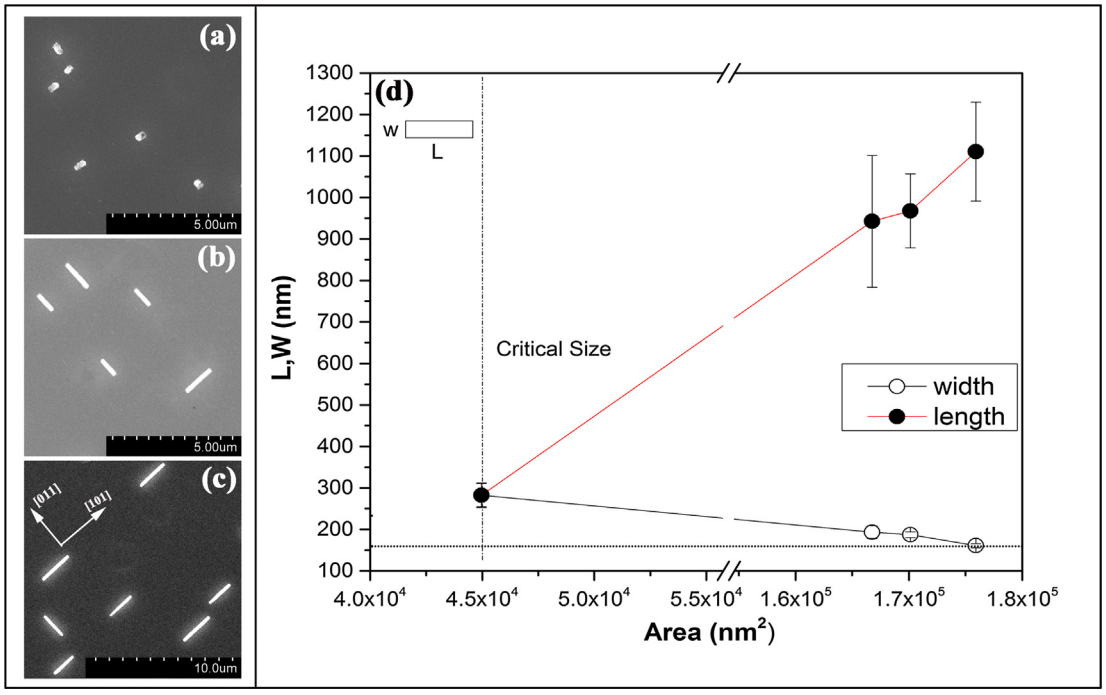

Fig. 6. Three stages of Cu_3Si island growth on a p-type Si(1 1 1) substrate as seen with SEM: (a) square islands, (b) rectangular islands, and (c) long, wire-shaped islands. Panel (d) shows the dependence of both island length L(closed circles) and width W(open circles) on the island surface area.

From this plot, one can see that the island nucleation density increases with time up to 3 ML (each minute corresponds to one ML of deposition) before reaching a saturation value. With further deposition, the density decreases and the area of the islands increases. This can be interpreted in terms of the probability of deposited "free" atoms being captured by existing islands versus forming the nucleation points for new islands. Beyond the 3 ML deposition point, the capture probability is higher and the island density decreases due to coalescence, i.e existing islands grow larger until they touch each other.

4. Conclusion

We have presented experimental data on the formation of Cu_3Si nanoislands on three Si substrates. In all cases, the initial island nucleation relies on the formation of voids in a native oxide on the substrates that are prepared by sustained annealing. Within the limits of

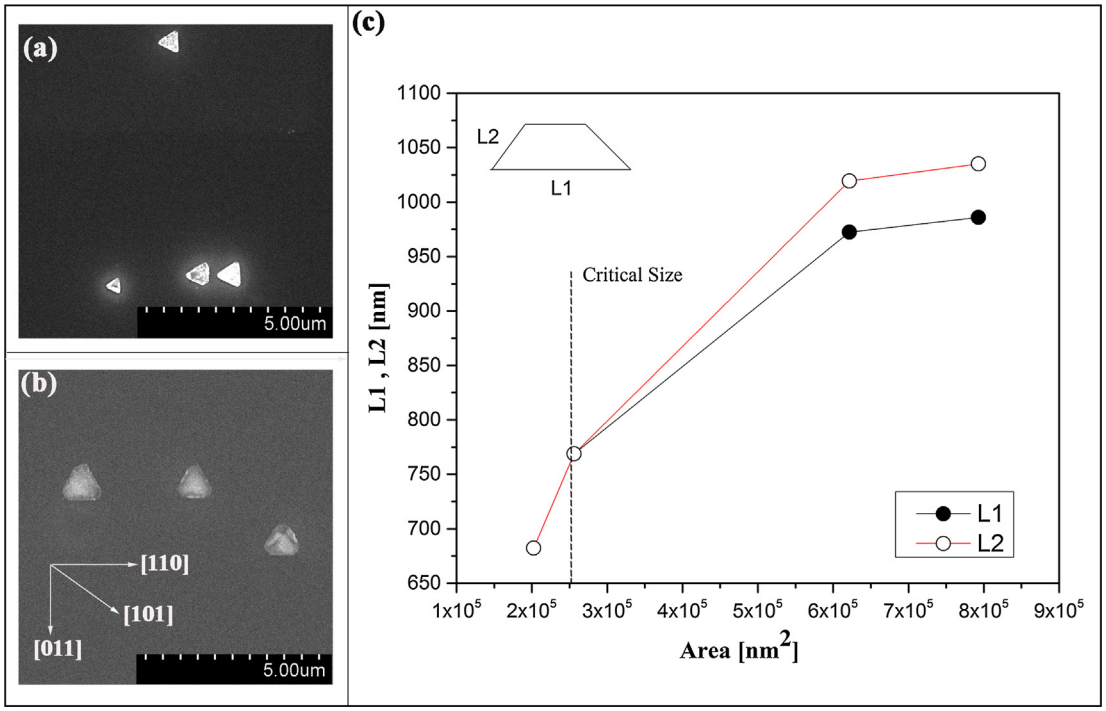

Fig. 7. Two stages of Cu_3Si island growth on an n-type Si(1 1 1) substrate as seen with SEM: (a) triangular islands and (b) trapezoidal islands. Panel (c) shows the dependence of the lengths L1 and L2 on the island surface area.

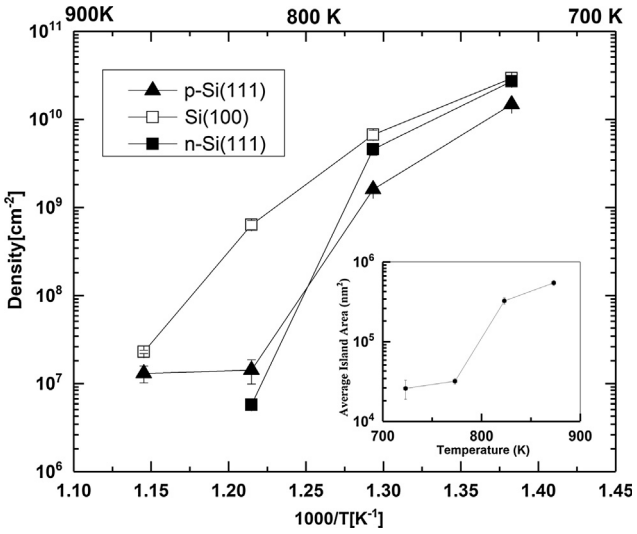

Fig. 8. A plot of the measured island density on three different substrates as a function of inverse temperature. The inset shows the average area of islands for these substrates across this temperature range. These depositions were performed at a rate of 1 ML/minute.

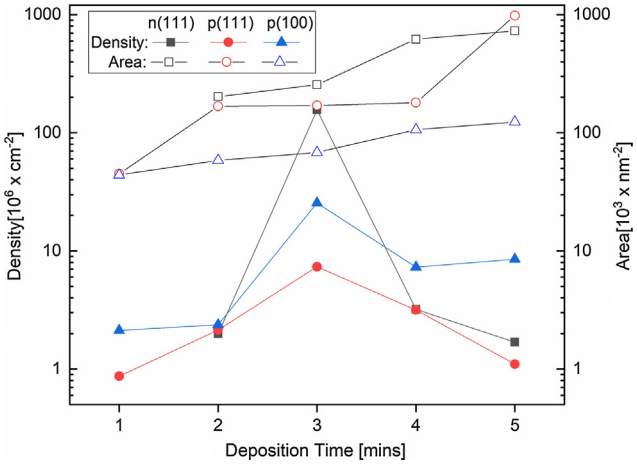

Fig. 9. A plot of the measured island density and the average area of islands as a function of the deposition time for Cu on the three different substrates studied.

our SEM imaging, the void density depends linearly on the temperature at which the anneal is performed. While different island shapes were observed, these were specific to the substrate under study and consistent with the underlying symmetry of the substrate. In addition, all islands underwent a growth and shape transition beyond a certain dimensional limit or critical size. This shape change is related to a model put forth by Tersoff and Tromp that addresses energy minimization through a shape transition [27].

References

[1] N.C. Cirillo, H.K. Chung, P.J. Vold, M.K. Hibbsbrenner, A.M. Fraasch, J. Vac. Sci. Technol. B 3 (6) (1985) 1680.
[2] S.P. Murarka, J. Vac. Sci. Technol. 17 (1980) 775.
[3] J.X. Xu, R.H. Yao, K.W. Geng, J. Vac. Sci. Technol. A 29 (2011) 051202.
[4] F. Deng, R.A. Johnson, P.M. Asbeck, S.S. Lau, W.B. Dubbelday, T. Hsiao, J. Woo, J. Appl. Phys. 81 (1997) 8047.
[5] H. Iwai, T. Ohguro, S. Ohmi, Microelectron. Eng. 60 (2002) 157.
[6] C. Ryu, K.W. Kwon, A.L.S. Loke, H. Lee, T. Nogami, V.M. Dubin, R.A. Kavari, G.W. Ray, S.S. Wong, IEEE Trans. Electron Devices 46 (1999) 1113.
[7] P. Kapur, J.P. McVittie, K.C. Saraswat, IEEE Trans. Electron Devices 49 (2002) 590.
[8] M. Lane, R.H. Dauskardt, N. Krishna, I. Hashim, J. Mater. Res. 15 (2000) 203.
[9] T. Osaka, N. Takano, T. Kurokawa, T. Kaneko, K. Ueno, J. Electrochem. Soc. 149 (2002) C573.
[10] T.Y. Kim, H.J. Son, S.K. Lim, Y.I. Song, H.S. Park, S.J. Suh, J. Nanosci. Nanotechnol. 14 (2014) 9515.
[11] Y. Cechal, J. Polcak, M. Kolibal, P. Babor, T. Sikola, Appl. Surf. Sci. 256 (2010) 3636.
[12] Z. Zhang, L.M. Wong, H.G. Ong, X.J. Wang, J.L. Wang, S.J. Wang, H. Chen, T. Wu, Nano Lett. 8 (2008) 3205.
[13] S. Li, H. Cai, C.L. Gan, J. Guo, Z. Dong, J. Ma, Crys. Growth Des. 10 (2010) 2983.
[14] P.-K. Ng, J.-Y. Cheng, B. Fisher, C. Lilley, Nanotechnology Materials and Devices Conference (NMDC), 2012, IEEE, 2012, p. 67.
[15] Y.T. Bie, J.L. Yu, J. Yang, W. Lu, Y.N. Nuli, J.L. Wang, Electrochim. Acta 178 (2015) 65.
[16] J.B. Zhou, N. Lin, Y. Han, J. Zhou, Y.C. Zhu, J. Du, Y.T. Qian, Nanoscale 7 (2015) 15075.
[17] K. Xu, Y. He, L. Ben, H. Li, X. Huang, J. Power Sources 281 (2015) 455.
[18] K.Q. Xu, Y. He, L.B. Ben, H. Li, X.J. Huang, J. Power Sources 281 (2015) 455.
[19] F.W. Yuan, C.Y. Wang, G.A. Li, S.H. Chang, L.W. Chu, L.J. Chen, H.Y. Tuan, Nanoscale 5 (20) (2013) 9875.
[20] S.A. Chaparro, Y. Zhang, J. Drucker, D. Chandrasekhar, D.J. Smith, J. Appl. Phys. 87 (2000) 2245.
[21] J. Wu, P. Jin, Frontiers Phys. 10 (2015) 7.
[22] A.M. Yaremko, V.M. Dzhagan, P.M. Lytvyn, V.O. Yukhymchuk, M.Y. Valakh, Phys. Status Solidi B 242 (2005) 2833.
[23] S.H. Brongersma, M.R. Castell, D.D. Perovic, M. Zinke-Allmang, Phys. Rev. Lett. 80 (1998) 3795.
[24] H.F. Hsu, T.F. Chiang, H.C. Hsu, L.J. Chen, Jpn. J. Appl. Phys., Part 1 43 (2004) 4541.
[25] J.C. Mahato, D. Das, R.R. Juluri, R. Batabyal, A. Roy, P.V. Satyam, B.N. Dev, Appl. Phys. Lett. 100 (2012) 263117.
[26] K. Sekar, G. Kuri, P.V. Satyam, B. Sundaravel, D.P. Mahapatra, B.N. Dev, Phys. Rev. B 51 (1995) 14330.
[27] J. Tersoff, R.M. Tromp, Phys. Rev. Lett. 70 (1993) 2782.
[28] D.E. Jesson, G. Chen, K.M. Chen, S.J. Pennycook, Phys. Rev. Lett. 80 (1998) 5156.
[29] J.L. McChesney, A. Kirakosian, R. Bennewitz, J.N. Crain, J.L. Lin, F.J. Himpsel, Nanotechnology 13 (2002) 545.
[30] D. Lee, S. Kim, Appl. Phys. Lett. 82 (2003) 2619.
[31] Y. Chen, D.A.A. Ohlberg, R.S. Williams, J. Appl. Phys. 91 (2002) 3213.
[32] C. Preinesberger, G. Pruskil, S.K. Becker, M. Dahne, D.V. Vyalikh, S.L. Molodtsov, C. Laubschat, F. Schiller, Appl. Phys. Lett. 87 (2005) 083107.
[33] Y. Chen, D.A.A. Ohlberg, G. Medeiros-Ribeiro, Y.A. Chang, R.S. Williams, Appl. Phys. Lett. 76 (2000) 4004.
[34] J. Nogami, B.Z. Liu, M.V. Katkov, C. Ohbuchi, N.O. Birge, Phys. Rev. B 63 (2001) 233305.
[35] R. Ragan, Y. Chen, D.A.A. Ohlberg, G. Medeiros-Ribeiro, R.S. Williams, J. Cryst. Growth 251 (2003) 657.
[36] D. Lee, D.K. Lim, S.S. Bae, S. Kim, R. Ragan, D.A.A. Ohlberg, Y. Chen, R.S. Williams, Appl. Phys. Mater. Sci. Process. 80 (2005) 1311.
[37] L.J. Chen, K.N. Tu, Mater. Sci. Rep. 6 (1991) 53.
[38] K.C.R. Chiu, J.M. Poate, J.E. Rowe, T.T. Sheng, A.G. Cullis, Appl. Phys. Lett. 38 (1981) 988.
[39] S.Y. Chen, L.J. Chen, Appl. Phys. Lett. 87 (2005) 253111.
[40] Z.A. He, D.J. Smith, P.A. Bennett, Phys. Rev. Lett. 93 (2004) 256102.
[41] S.Y. Chen, H.C. Chen, L.J. Chen, Appl. Phys. Lett. 88 (2006) 193114.
[42] N. Benouattas, A. Mosser, D. Raiser, J. Faerber, A. Bouabellou, Appl. Surf. Sci. 153 (2000) 79.
[43] R.R. Chromik, W.K. Neils, E.J. Cotts, J. Appl. Phys. 86 (1999) 4273.
[44] J.A. Venables, G.D.T. Spiller, M. Hanbucken, Rep. Prog. Phys. 47 (1984) 399.